Search for the heaviest atomic nuclei among the products from reactions of mixed-Cf with a ^{48}Ca beam

N. T. Brewer *et al.*

Phys. Rev. C **98**, 024317 — Published 24 August 2018

DOI: 10.1103/PhysRevC.98.024317

Search for the heaviest atomic nuclei among the products from reactions of mixed-Cf with a ^{48}Ca beam

N. T. Brewer[1,2,3,†], V. K. Utyonkov[4] , K. P. Rykaczewski[2] , Yu. Ts. Oganessian[4] , F. Sh. Abdullin[4] , R. A. Boll[2], D. J. Dean[2], S. N. Dmitriev[4] , J. G. Ezold[2] , L. K. Felker[2] , R. K. Grzywacz[2,3] , M. G. Itkis[4] , N. D. Kovrizhnykh[4] , D. C. McInturff[2], K. Miernik[1,5] , G. D. Owen[2] , A. N. Polyakov[4] , A. G. Popeko[4] , J. B. Roberto[2] , A. V. Sabel'nikov[4] , R. N. Sagaidak[4] , I. V. Shirokovsky[4] , M. V. Shumeiko[4] , N. J. Sims[2] , E. H. Smith[2] , V. G. Subbotin[4] , A. M. Sukhov[4] , A. I. Svirikhin[4] , Yu. S. Tsyganov[4] , S. M. Van Cleve[1] , A. A. Voinov[4] , G. K. Vostokin[4] , C. S. White[2] , J. H. Hamilton[6] , M. A. Stoyer[7]

[1] *JINPA, Oak Ridge National Laboratory, Oak Ridge, TN 37831, USA*

[2] *Oak Ridge National Laboratory, Oak Ridge, Tennessee 37831, USA*

[3] *Department of Physics and Astronomy, University of Tennessee, Knoxville, Tennessee 37996, USA*

[4] *Joint Institute for Nuclear Research, RU-141980 Dubna, Russian Federation*

[5] *Faculty of Physics, University of Warsaw, PL-02-093 Warsaw, Poland*

[6] *Department of Physics and Astronomy, Vanderbilt University, Nashville, Tennessee 37235, USA*

[7] *Lawrence Livermore National Laboratory, Livermore, California 94551, USA*

[†] *brewernt@ornl.gov*

(Dated: August 1, 2018)

The search for new decay chains of oganesson isotopes is presented. The experiment utilized the Dubna Gas Filled Recoil Separator and a highly segmented recoil-decay detection system. The signals from all detectors were analyzed in parallel by digital and analog data acquisition systems. For the first time, a target of mixed californium (51% ^{249}Cf, 13% ^{250}Cf and 36% ^{251}Cf) recovered from decayed ^{252}Cf sources was produced and irradiated with an intense ^{48}Ca beam. The observation of a new decay chain of ^{294}Og is reported. The prospects for reaching new isotopes ^{295,296}Og are discussed.

I. INTRODUCTION

The seventh row of the Periodic Table spanning the atomic numbers $Z = 87$ and $Z = 118$ has been completed with the recent discoveries and namings of the elements $Z = 113$ nihonium, $Z = 115$ moscovium, $Z = 117$ tennessine and $Z = 118$ oganesson [1]. The decay properties of the heaviest synthesized nuclei provide an indication of enhanced stability due to shell correction energy and that the edge of the "long sought island of stability"[2] has been reached [2, 3]. However, many of the overarching questions related to studies of superheavy atoms and nuclei are still not answered. The predictions regarding the extent of the Periodic Table [4] and of the Segre Chart of Nuclei differ dramatically, as in Ref. [5], for example. Nuclear structure models usually point to the magic character of neutron number, $N = 184$, but do not agree on a specific proton number enhancing stability. The strong Coulomb field in superheavy nuclei, and in $Z = 118$ oganesson isotopes in particular, affects the proton and neutron densities and shell structure, see [6–8] and references therein. In some calculations, this "Coulomb frustration" can cause a depression in the proton density in the center of oganesson isotopes [7]. As the 118th element, oganesson is placed in the group of noble gases. However, in contrast to other elements in group 18, it is predicted to be solid at room temperature, see [6] and refs therein.

Calculations of the production yields of new elements and nuclei strongly rely on nuclear structure input, in particular, on the fission barrier analysis. New data on even heavier nuclei are needed to verify these predictions and select the models most capable to give reliable guidance to future discovery experiments.

The production of the heaviest target materials is a very important technical development enabling studies synthesizing heavier nuclei. There was a several month chemical separation campaign at the Radiochemical Engineering Development Center (REDC) at Oak Ridge National Laboratory (ORNL) to recover the various Cf isotopes from decades old ^{252}Cf sources. These sources were originally dominated by highly radioactive ^{252}Cf ($T_{1/2} =$ 2.6 y), but after three decades about 16 milligrams of a mixture of ($Z = 98$) californium material with the abundances shown in Table I was recovered. The ^{251}Cf content is the heaviest target isotope used for the search of new superheavy nuclei [9]. This Cf-material is therefore valuable for answering basic science questions about the

limits of nuclear existence. The target preparation and the results of the first attempt of irradiations with ^{48}Ca beam performed at the Dubna Gas Filled Recoil Separator (DGFRS) are presented here. The average properties of the ^{294}Og decay chain identified among the reaction products are compared to theoretical predictions and previous results. The possibility of reaching new heavier isotopes ^{295}Og and ^{296}Og is discussed.

II. REVIEW

A. Earlier experiments on ^{294}Og

The first identification of an isotope of element 118, now known as oganesson, was attempted and successful at JINR Dubna in 2002 using the ^{249}Cf+^{48}Ca reaction [10]. The ^{48}Ca beam energy was selected above the Coulomb barrier to create the ^{297}Og compound nucleus with an excitation energy of E^* of about 29 MeV. With an accumulated beam dose of 2.5×10^{19} particles of ^{48}Ca at 245 MeV, a single decay chain of recoil tagged and correlated high energy alpha decays and spontaneous fission (recoil-α-α-SF) was detected. By comparing the theoretically predicted and observed decay properties, the assignment of ^{294}Og was proposed for the new parent activity. Further direct synthesis of $Z = 114$ and $Z = 116$ decay products of ^{294}Og confirmed the initial interpretation [11, 12]. The estimated cross section for the $3n$ reaction channel based on one observed event was $0.3^{+1.0}_{-0.27}$ pb. In addition, one SF event with high energy of fission fragments and decay time of 3.2 ms was observed and its possible assignment to ^{294}Og decay was discussed.

The second experiment with a ^{249}Cf target and ^{48}Ca beam was performed in 2005 at a higher beam energy of 251 MeV corresponding to the compound nucleus excitation energy range between 32 MeV and 37 MeV. Two additional events consistent with the first decay chain were detected, and the properties of all three decay chains attributed to ^{294}Og decay were presented in [13]. The half-life of ^{294}Og based on three α decays at the average energy of 11.65 ± 0.06 MeV was determined to be $0.89^{+1.07}_{-0.31}$ ms. Two decay chains consisted of recoil-α-α-SF events and one longer decay chain terminated with SF after three consecutive α decays. These observations are consistent with independently studied decay properties of the grand-daughter isotope of ^{294}Og, ^{286}Fl, with similar decay probabilities through α emission and spontaneous fission. The cross section at the beam energies used to observe these two new ^{294}Og events was estimated to be $0.5^{+1.6}_{-0.3}$ pb for the excitation energy range $E^* = 32.1$-36.6 MeV [13].

Long irradiations of ^{249}Bk from ORNL with ^{48}Ca were performed throughout 2009-2012 at JINR in Dubna yielded the identification of a new element, with 117 protons, known now as tennessine as well as an observation of one event of ^{294}Og [14]. The isotope ^{249}Bk beta decays with a half-life of 327 days [15] to ^{249}Cf. This is comparable to the time taken for the target transportation and production as well as for long target irradiations at the DGFRS. The recoil-α-α-SF decay chain observed during the experiment with initially pure ^{249}Bk material has properties which are in agreement with earlier established decay properties of ^{294}Og. The cross section estimate for this single event of $0.3^{+0.7}_{-0.26}$ pb for the excitation energy range of $26.6 - 37.5$ MeV for ^{297}Og was also in good agreement with earlier deduced cross sections. The four-event average of ^{294}Og decays yielded $T_{1/2}$ of $0.69^{+0.64}_{-0.22}$ ms and $E_\alpha = 11.66 \pm 0.06$ MeV [14]. The observation of a decay chain of ^{294}Og in the experiment on tennessine isotopes with a mixed ^{249}Bk/^{249}Cf target offers additional confirmation of the consistency of superheavy nuclei identification at the DGFRS. A summary of decay properties as they were experimentally known prior to this campaign is shown in Fig. 1.

TABLE I. Original and recovered Cf isotope content.

Isotope	Half-life	Percent as produced	Percent as shipped in 2015	Mass in 2015 (mg)
^{249}Cf	351 y	3.41	50.6	5.61
^{250}Cf	13.08 y	8.7	13.1	1.45
^{251}Cf	898 y	2.6	36.3	4.03
^{252}Cf	2.645 y	85.27	0.02	0.002
^{253}Cf	0.049 y	0.004	-	-
^{254}Cf	0.166 y	0.010	-	-

B. Theoretical Predictions

While theoretical predictions in the extremity of known nuclear matter are poorly constrained experimentally, helpful conclusions can still be drawn from an understanding of the relevant physics and can give a perspective for experimental feasibility. In Table II, an overview of theoretical approaches modeling relevant target, projectile and/or exit channel systematics for the production of Og isotopes in the reactions between ^{48}Ca and different long lived Cf isotopes are shown. These models provide the maximum evaporation residue cross-section (ERCS) listed in picobarns and the corresponding excitation energy in the compound nucleus (E^*_{CN}) in units of MeV. For those references [16, 17] which quote values in the center-of-mass frame, the masses from [18] have been used for conversion. This maintains consistency with references [19–22] which are using masses from [18] and do not differ from the current evaluation [23] when based upon experimental numbers. The predicted cross-sections across the listed parameter space varies between 1 fb and 100 pb. However, various theoretical approaches show some similar trends.

The frameworks listed all tend to show the highest ERCSs for $3n$ and $4n$ emission with the exception of Ref. [17] which would show a $5n$ preferred channel from reac-

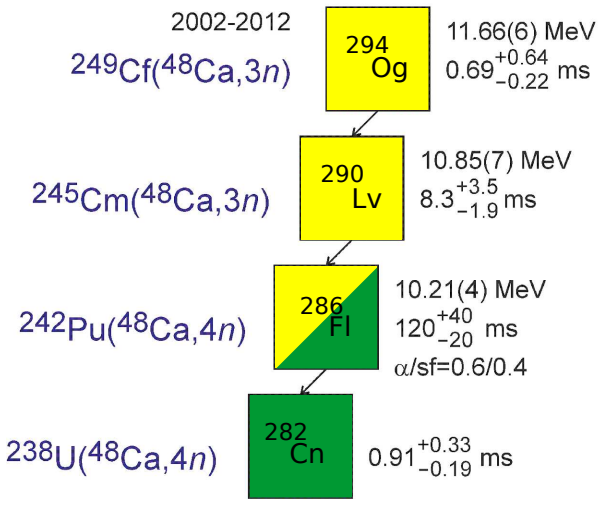

FIG. 1. The summary of the decay properties from the synthesis of ^{294}Og and all of the observations of its progeny. Numbers in parenthesis next to the energy indicate the weighted average of previous results quoting the uncertainty as the FWHM for the energy resolution.

tions of ^{48}Ca on ^{252}Cf and that of Ref. [21] which slightly favors the $2n$ exit channel on ^{251}Cf. The models also show some agreement for the maximum E^*_{CN} which would lead to peak ERCS. There is a 6-10 MeV difference between exit channel maxima with the value in Ref. [24] being about 5 MeV lower than those of Refs. [16, 17] and those of Ref. [21] being 10-15 MeV lower. Importantly, most approaches agree that reactions are more likely on either ^{249}Cf or ^{251}Cf. These are the isotopes which are most abundant in the target used for the experiment. When folded with the isotopic abundance in the target material the likely synthesis can be assessed as well. From the calculations shown in Ref. [24] ^{294,295,296}Og would be equally likely, from Ref. [21], production of ^{294}Og and ^{295}Og is most likely depending on inputs to the model and there is favored synthesis in Ref. [16] for ^{296}Og. The calculation from Ref. [17] is for a mixed Cf target (abundance percentages were slightly different than the final ones in our mixed-Cf target). The conclusion given is that synthesis of ^{295}Og is most probable with ^{294}Og and ^{293}Og following and this general conclusion persists considering the abundance percentages of the target material used. The result from [25] suggests ^{293}Og and ^{294}Og as preferred channels depending on the energy of the compound nucleus, but the consideration of individual exit channel was not listed.

Further considered, but not shown in Table II, are references [19, 20, 22] which include predictions about reactions on ^{249}Cf. Significant effort is given in [22] to detail the effect of various inputs on the reaction and shows 1 pb or greater ERCS's for the favored $3n$ exit channel. If references [19, 26] are taken together this also gives a positive outlook on the possibility of running with ^{48}Ca on ^{249}Cf and ^{251}Cf, indicating $3n$ neutron evaporation as most likely and producing both ^{294}Og and ^{296}Og with ERCSs of around 1 pb.

In summary, various theoretical approaches indicate that ^{294}Og, ^{295}Og and ^{296}Og are expected in reactions of ^{48}Ca on a mixed californium target within a reasonable experimental time frame. There is also reasonable guidance for the excitation energy that could be used to increase the probability of success. These three products would be distinguishable from each other utilizing the typical α-α-SF-time correlation method because daughter isotopes ^{290}Lv, ^{291}Lv and ^{292}Lv and their decays are already known [3].

III. MIXED-CF TARGET

A. Preparation of mixed-Cf target at the ORNL REDC and assembly at JINR

In brief, with more details contained in [9], the REDC at ORNL has continued [27–30] to provide unique capabilities for the production of target material intended for use in studies of superheavy element synthesis. It was recognized that aged californium sources, in some cases more than 40 years, would provide a good source of target material for superheavy element (SHE) experiments due to its relative enrichment of isotopes with longer half-lives than that of ^{252}Cf. With all sources having aged more than 30 years, significant decay of the ^{252}Cf content resulted in californium material having a lower neutron flux, which was then manageable for use in shielded glove boxes.

Approximately 16 mg of mixed Cf were recovered from the aged sources with an isotopic composition as listed in Table I. Only enough Cf material for two target segments, about 2 mg, was moved into the shielded processing glove box at one time in order to limit exposure. The shield, located on the front of the glove box, consisted of three inches of leaded acrylic. The target segments, using Teflon coated anodized aluminum framing and titanium deposition foils 1.6 μm thick, were fully assembled prior to the electrodeposition process in order to minimize handling of the extremely thin foil after deposition. The electrodeposition well made of polyether ether ketone (PEEK) and sealed with silicon gaskets was designed to hold the fully assembled target segment inserted into one side (cathode) and a thicker titanium foil (anode) inserted on the other side. A total of 17 isobutanol electrodepositions were performed with 5 resulting target segments discarded due to deposition inhomogeneity, foil tearing, or contamination. The 12 viable segments had an average Cf layer thickness of 309 μg/cm^2 and a total neutron rate of 2×10^7 n/s. A deposition efficiency of more than 80% in all segments was achieved.

In February 2015, the 12 segments, each segment containing 1 mg mixed Cf, were packaged into 6 drums and shipped to JINR. There they were mounted into a target

TABLE II. Theoretical predictions of excitation energy in the compound nucleus (E^*_{CN}, MeV) for an optimum evaporation residual cross-section (ERCS, pb unless stated otherwise) associated with given neutron evaporation channel (xn) from five models analyzing reactions of ^{48}Ca on $^{249-252}$Cf producing $^{292-298}$Og.

Target	xn	A_{ER}	E^*_{CN}[a]	ERCS[a]	E^*_{CN}[b]	ERCS[b]	E^*_{CN}[c]	ERCS[c]	E^*_{CN}[d]	ERCS[d]	E^*_{CN}[e]	ERCS[e]
249	2	295			27/22	0.2/2			29	0.12	32.2	0.26[f]
	3	294	35	0.1	28/28	1 / 6	38	9.8	38	0.32		
	4	293	42	0.06	36/36	0.3/0.5	48	1.1	48	0.6		
	5	292	50	0.04	44/44	4/5 fb			58	0.14		
250	2	296			26/23	1 / 10			29	0.15	33.4	0.18[f]
	3	295	36	0.02	28/28	4 / 20	37	21.9	38	3.1		
	4	294	42	0.1	35/33	0.4/0.9	48	2.1	48	1.3		
	5	293			43/43	2/2 fb			57	0.65		
251	2	297			23/23	1 / 3			29	0.03	34.2	0.38[f]
	3	296	34	0.2	27/26	0.8 / 6	39	36.4	38	0.08		
	4	295	40	0.2	35/34	.2/.7	47	4.7	48	0.35		
	5	294			42/42	.015/.2			57	0.04		
252	2	298			24/24	0.3 / 2			28	0.005	36	0.15[f]
	3	297	33	0.06	28/28	1 / 9	38	81.4	38	0.055		
	4	296	40	0.5	34/34	0.5/2	48	12.4	48	0.045		
	5	295			41/41	0.04/0.05	58	1.5	57	0.075		

[a] Reference [24].
[b] Reference [21].
[c] Reference [16].
[d] Reference [17].
[e] Reference [25].
[f] Total ERCS.

wheel behind heavy shielding.

B. Dubna Cf-target wheel arrangement and its assembly procedure and shielding

In a glove box, the target disk was mounted in a holder which was closed by borated polyethylene with a thickness of 3 cm from all sides with the exception of a hole for mounting one sector. When the next sector was attached to the target disk, the disk was turned to install the next sector. Finally, the disc with 12 target sectors in the same glove box was placed into the target block.

IV. THE EXPERIMENT AT THE DGFRS

Beginning in the fall of 2015 and continuing through early 2016 an experiment was performed at the DGFRS with reactions of ^{48}Ca on the mixed-Cf target. The first phase of this experiment was performed from October 1st through December 28th 2015 at a beam energy of 252 MeV in the laboratory frame, corresponding to an excitation energy in the compound nucleus of 35.2 ± 2.2 MeV and 36.4 ± 2.2 MeV for target reactants ^{249}Cf and ^{251}Cf respectively. The beam energy is measured with a time-of-flight system which has a systematic uncertainty of 1 MeV. A total beam dose of 1.6×10^{19} was put on target. Phase two was conducted from February 10th 2016 and concluded on April 6th 2016. The beam energy was increased to 258 MeV in order to observe other exit channels. This produced an excitation energy of 40.1 ± 2.3 MeV and 41.3 ± 2.3 MeV for ^{249}Cf and ^{251}Cf respectively. The higher energy would likely favor $4n$ over $3n$ emission. In total, a beam dose of 1.1×10^{19} was achieved during this phase.

Characterization and calibration of the detectors and target condition was achieved via the reactions of ^{48}Ca on ^{nat}Yb, ^{48}Ca on ^{206}Pb and alpha emission from the radioactive Cf target. The reaction of ^{nat}Yb on ^{48}Ca produces $^{216-220}$Th in highest abundance and provides robust characterization of the capabilities of the detection system first reported in [31]. This reaction is used to fine tune the acquisition settings especially for the multiwire proportional counters (MWPCs) in order to provide low thresholds and dead times. Spontaneous fission (SF) activity is calibrated with the use of ^{48}Ca on ^{206}Pb producing ^{252}No. The performance of the target was monitored periodically throughout the experiment by acquiring count rates and spectra of alpha particle emission from the rotating mixed-Cf target by correlating with the position of the target using a timing signal from photo-diodes shining through a slot mounted on the rotation shaft of the target wheel.

A. Description of the focal plane detection system

After the fusion reaction takes place, the resultant product is separated from beam particles, scattered ions, and transfer-reaction products in the DGFRS. Afterwards, the ions are tagged with a time-of-flight (TOF) in two pentane filled MWPCs at a pressure of 1.5 Torr. The counters are placed 65 mm apart and are separated from the DGFRS volume by a 0.2 mg/cm^2 Mylar film.

A new focal plane detection array has been designed, assembled, and commissioned at ORNL, then implemented and further characterized at the DGFRS at JINR. It consists of a double-sided silicon strip detector (DSSD), surrounded by a silicon box for the detection of escaped alphas and a veto detector placed behind for additional rejection of light particles. The DSSD is a single 300-micron thick silicon wafer (model BB-17) manufactured by Micron Semiconductor, Ltd. The strips are 1 mm wide and there are 48 horizontal strips on the front side and 128 vertical strips on the back side. This creates a high pixelation for position resolution and is used to reduce the per pixel (of which there are 6144) rate of recoil-decay events and reduces the probability for random correlations. There are six Si detectors which form an escape capture box. There are two Si on the top and bottom of the DSSD and one detector on each side. Each detector is a model MSX-7200 and each is 65 mm by 120 mm and 500 microns thick. The orientation is such that each detector extends 120 mm perpendicular to the DSSD face in the direction of the incoming beam. Additionally, a single Si veto detector (MICRON MSX-62) backs the DSSD as an active veto of events which pass through the DSSD. The 500-micron thick detector matches the width and height of the DSSD and is mounted on an identical frame and placed at a distance of 3 mm behind the implantation DSSD.

Each silicon detector signal is first passed through MESYTEC linear preamplifiers (MPR-64). Room and preamplifier temperature are continually recorded for gain correction if necessary. During this campaign preamplifier temperature variation from the mean was less than $\pm$ 0.5 $^{\circ}C$ and no correction was needed or applied. After the preamplification stage, the signals are split into two branches: analog and digital.

The analog branch is similar to the one described in [32] and it is tied into control systems for the automatic deflection of the beam in the case of a correlation of interest. Because daughter products may be long lived, it is important to have detection of later decays free from beam-induced background. In the case that no latter decays are identified within a prescribed window, the beam is automatically returned to irradiate the target.

The digital branch is instrumented by 13 Pixie-16 DGFs from XIA running in a hybrid analysis mode. This mode is one for which signals with a time difference greater than 10 μs are passed through an onboard filtering scheme for time and energy identification. If the fast (timing) filter detects pulses within 10 μs of one another, the pulses are recorded for analysis in software. Because of its fast clock, the digital system is used especially for its high efficiency tagging of recoils in the MWPC and sensitivity to the shortest half-lives. Analysis was performed with the following frameworks [33–37]. Examples are shown below. In general, use of this new detection system resulted in a better energy resolution and lower energy thresholds for recorded signals [31, 51].

B. The performance of the new fast-detection system and analysis of the digital data branch

Prior to experiments with ^{48}Ca beams and actinide targets producing SHE, calibrations require alpha particles at large energies in order to provide the closest calibration to the energy range of alpha particles emitted from elements of much higher proton number. External sources are not used due to various energy loss mechanisms. Instead, the reaction ^{48}Ca + ^{nat}Yb is used for calibration with implanted activities. This fusion-evaporation reaction on several Yb isotopes (with masses A = 170,171,172,173,174 and 176 and abundances of 3%, 14%, 22%, 16%, 32%, and 13%, respectively) creates a range of $Z = 90$ thorium isotopes, which due to their proximity to the $N = 126$ shell closure have alpha energies near 10 MeV. These radioactive Th isotopes (with mass number ranging from 214 to 221) are implanted into silicon detectors allowing us to record the full decay energy of alpha emission and nuclear recoil. The cross sections are large enough to collect statistics sufficient to calibrate the full area of the detector's 128 by 48 strips within a day.

This reaction is now shown to be further useful because several reaction products have comparably short half-lives and this may be helpful for experiments attempting to synthesize elements with $Z > 118$. It has also been discussed [31] that observation of short lived activities is important for distinguishing complete-fusion and multi-nucleon transfer products.

The correlation plot for alphas emitted by thorium isotopes and their daughters is shown in Fig. 2. These activities are those which have an implant registered by TOF in a pixel of the DSSD and are followed by a decay (without an intervening implant). The x-axis shows the energy of the first alpha in a correlated chain and the y-axis shows the energy(s) of any subsequent alphas. Two examples can be seen in the figure and demonstrate our sensitivity to microsecond and sub-microsecond activities and the operation of the custom hybrid mode acquisition scheme [34, 38]. In the first case, ^{220}Th with a half-life of 9.7 μs [39] is registered as an implantation in the DSSD, this is followed by an α-α pileup (8.8 MeV and then 9.3 MeV) which then triggers the recording of a trace because, the half-life of this decay is 0.17 $\pm$ 0.05 μs [40]. It is also possible that all three pulses (ER-α-α) are recorded in the trace. In the second case, ^{219}Th is identified. Identification is defined in this case as a first alpha

between 9 and 10 MeV and a second between 8.2 and 9.2 MeV. Upper bounds of time differences are 10 μs and 10 ms, respectively. A recoil-α pileup is recorded and has a time difference distribution with a 0.94 ± 0.08 μs half-life. The reliable analysis of pileup events starts from a 250 ns time difference between recoil and alpha signals. The decay curve is shown in Fig. 3 and agrees with the evaluated value of 1.05 ± 0.03 μs [41]. The second alpha is recorded with the energy filter in the Field Programmable Gate Array (FPGA) of the digitizer. The half-life for the correlated decays of ^{215}Ra is 1.66 ± 0.07 ms. Additionally, there is a suppression factor for short recoil-α times due to the roughly 1 μs time of flight through the separator. However, even with losses from several mechanisms, ^{218}Th with an evaluated half-life of 116 ± 13 ns [42–45], is still identifiable due to the ability to process digitized signals. In the current analysis, recoil-alpha decay times shorter than 250 ns were not included. Uncertainty estimates which are based on 11 events and shown in Fig. 4 are statistical [46, 47].

C. Observation and properties of ^{294}Og decay chain

Within the first 8 days after the start of the experiment with a ^{48}Ca beam dose of 1.0×10^{18} on target, there was a detection of a correlated decay sequence which was consistent with the previously observed ^{294}Og. This was more than 16 times lower dose than the total dose during a previous experiment observing two oganesson decay chains [13]. The details of this decay chain, terminating in the fission of ^{286}Fl, are shown in Fig. 5. All parts of the decay chain are in agreement with previous measurements. The new event lowers slightly the average half-life and increases slightly the average decay energy of ^{294}Og.

The recoil implantation and following decays were registered near the corner of our large area detector (at the crossing of strip 7 out of 48 and 126 out of 128). In an earlier experiment [13], one of two recoils of oganesson was detected on the opposite far side (strip 1 out of 12), and re-enforces that it is important to have a large area implantation and decay counter.

Additionally, at both ^{48}Ca energies, about 150 SF events with $T_{1/2} = 1.24^{+0.16}_{-0.14}$ ms and high energy release were observed. This activity may originate from ^{258}No ($T_{1/2} = 1.2 \pm 0.2$ ms [48]) because its yield as well as yields of several other identified transfer-reaction products, such as ^{253}Es and $^{252-254}$Fm, are in good agreement with relative cross sections measured for nuclei which were observed in the ^{248}Cm + ^{48}Ca reaction [49] as products which were the same number of nucleons away from ^{248}Cm. Therefore, one can argue that the 3.2 ms high-energy fission event observed in [10] potentially originated from ^{258}No.

Among these SF events, there were signals correlated with incoming recoil-like signals within the time range of the ^{294}Og half-life. We have inspected the possible assignment of some SF events to the fission of ^{294}Og. In the past, as well very recently [50], ^{294}Og was considered as a system consisting of doubly-magic ^{208}Pb and single magic $N = 50$, ^{86}Kr. These two components are well bound stable nuclei. One can envision that an asymmetric fission of ^{294}Og into ^{208}Pb and ^{86}Kr fragments might be somewhat enhanced.

However, especially since the decay time of ^{294}Og is not sufficiently different from ^{258}No decay, one cannot make an assignment to ^{294}Og activity based only on the half-life of SF events. The energy of SF events vary, since we detect sometimes only a partial energy of fission fragments. Such events are more likely to arise from the SF activity produced in a multi-nucleon transfer involving the Cf isotope in the target [31, 51]. The indistinguishability of complete-fusion from transfer reaction products provides motivation for an ionization chamber which would have a discrimination capability for the atomic number Z, placed before the implantation Si-counter. Construction and anticipated performance of such an ionization chamber based on gas electron multiplier (GEM) technology [52] was recently discussed [53].

D. Cf target performance and cross-section estimate

Similar to all previous experiments, the beam intensity was gradually increased from 0.05 to 0.75 pμA during about four days. Before irradiation and more than 30 times during the experiment, when the beam was stopped for change of ^{48}Ca material in the ion source of the U400 cyclotron, the alpha activity emitted from the Cf layer was measured by the DSSD. For their detection, the current in the quadrupole lenses was switched off and rigidity of the dipole magnet was reduced from 2.31 Tm, used in the main experiment, to 0.34 Tm which corresponds to a maximum transmission of Cf alpha particles though separator. Three alpha spectra, measured from the mixed Cf rotating target wheel with the detector system in the focal plane of DGFRS, are shown on the right part of Fig. 6; the spectra from the ^{249}Cf target (0.34 mg/cm^2) used in 2005 for producing ^{294}Og [13] are shown on the left part of Fig. 6 for comparison. In both cases alphas passed through the target layer, hydrogen in the DGFRS, Mylar widow, and pentane and were then registered by detectors calibrated by alpha activities from implanted nuclei. For the ^{249}Cf target, the shape of spectra became gradually narrower and then was practically unchanged after a beam dose of less than 10^{18} as illustrated in Fig. 6. Note, the low-energy part of spectrum was even larger for some other targets used in other experiments. This could be caused by evaporation of volatile contaminants from the target.

A comparable shape of $^{249-251}$Cf alpha spectra was observed before beginning of the experiment; it became somewhat narrower after a beam dose of about 10^{18} but the low-energy part remained. At this dose, the decay chain of ^{294}Og was observed. However, unlike the exper-

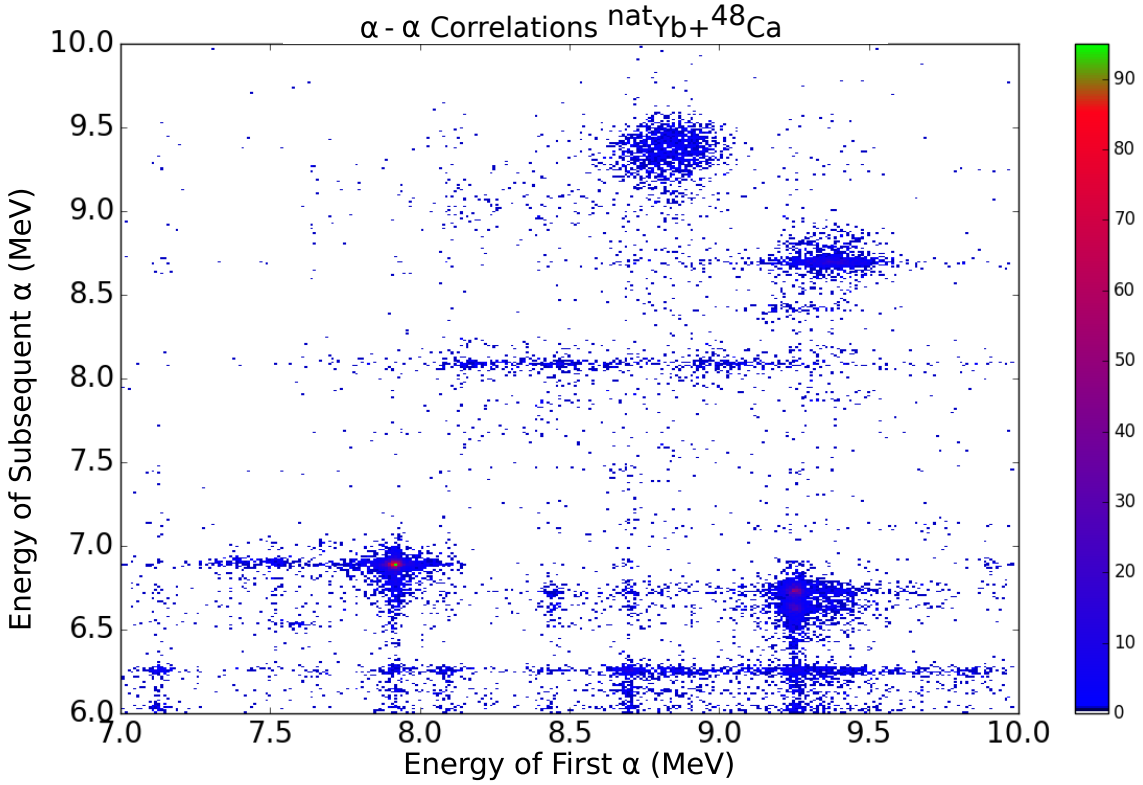

FIG. 2. Energies of alpha and subsequent alphas observed during the reaction of ^{nat}Yb + ^{48}Ca. ^{220}Th (8.8 MeV) $\rightarrow$^{216}Ra (9.3 MeV) and ^{219}Th (9.3 MeV) $\rightarrow$^{215}Ra (8.7 MeV) can be observed.

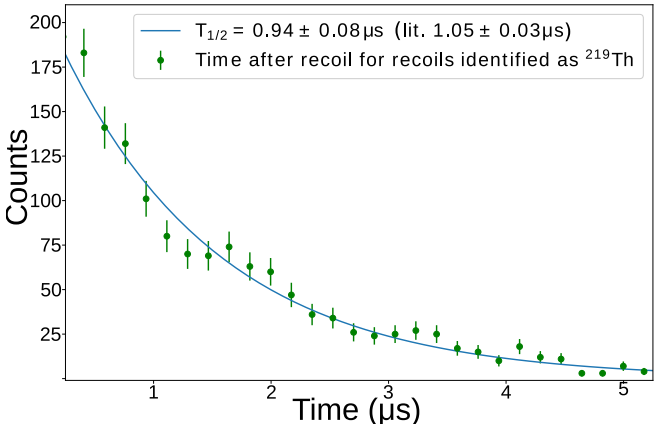

FIG. 3. Decay curve of ^{219}Th alpha decay observed at the DGFRS using the digital branch of the acquisition system during the ^{nat}Yb target irradiation with ^{48}Ca beam. Energies of ER had a distribution with an average (FWHM) of 6.2 (3.8) MeV. Analysis starts at time differences of 250 ns, see text.

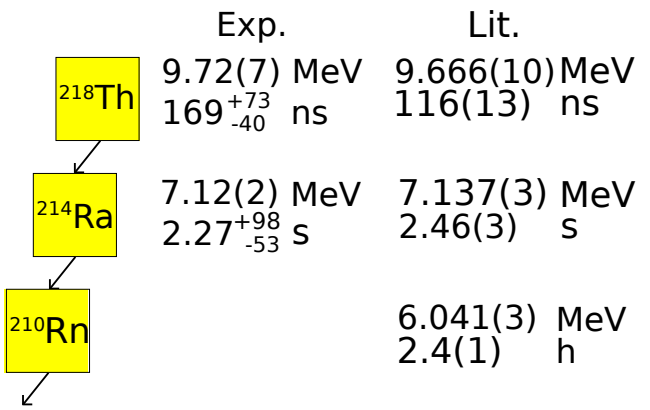

FIG. 4. Average decay properties of identified ^{218}Th recoils from the current work (11 events) as compared to values obtained from [42–45]. For comparison to the literature value, the uncertainty on the energy is the 1σ standard deviation. The energies of ER in the DSSD had an average (FWHM) of 6.6 (5.2) MeV.

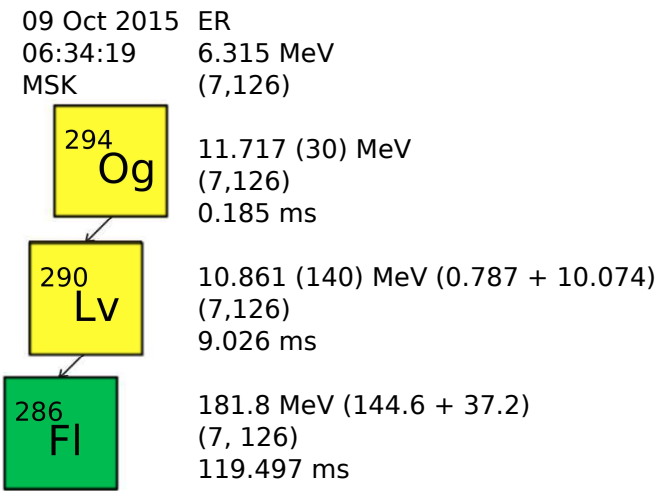

FIG. 5. Decay chain of ^{294}Og as observed in the digital acquisition on 09 October 2015. Uncertainties on the energy correspond to the FWHM of the resolution.

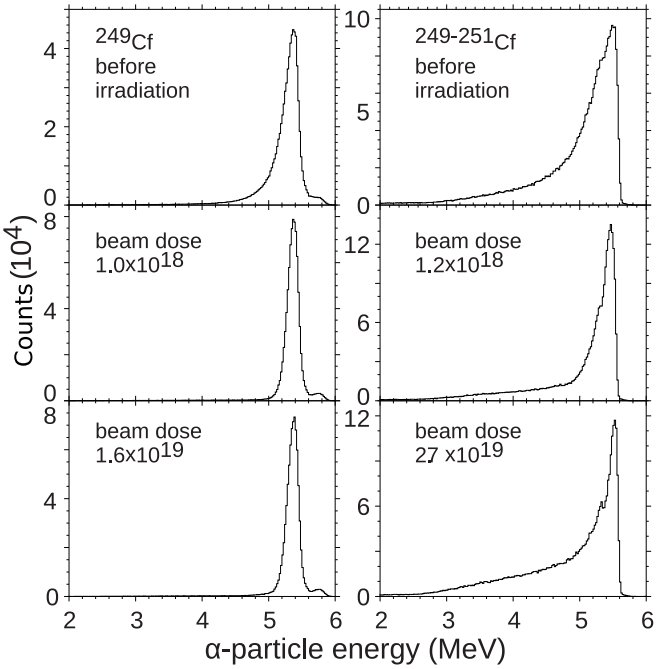

FIG. 6. Alpha spectra measured from the ^{249}Cf (left panel) and mixed-Cf (right panel) rotating targets with the detector system in the focal plane of DGFRS before irradiations and after given beam doses of ^{48}Ca projectiles passing through the targets.

iment with the ^{249}Cf target, as the beam dose increased, the low-energy part of the spectrum continued to grow gradually and shown in Fig. 6 is the spectrum of alphas at the end of irradiation. Moreover, the counting rate of events passing the DGFRS and registering in the MWPC increased from about 50 s^{-1} in the beginning of experiment to 300-350 s^{-1} in April, 2016. Additionally, the yields of transfer-reaction products, e.g., ^{246}Cf, ^{253}Es, $^{252-254}$Fm, and ^{258}No were noticeably higher than in previous experiments at DGFRS.

This evidence suggests that during the experiment the surface of the target was covered by a layer of some material that resulted in an increase of multiple scattering of recoils and a corresponding decrease of transmission for complete-fusion reaction products. In addition, the suppression factor for scattered nuclei and transfer-reaction products could decrease because of the widening of their angular distribution and larger penetration of these products into a forward corner of the DGFRS. A visual inspection of the target confirmed our suspicions. One sector of the target, prior to irradiation, is shown in Fig. 7 and Fig. 8 shows parts of three sectors as they appeared after the experiment was stopped. Usually the target after irradiation becomes somewhat deformed but has a shiny surface. Such parts can be seen in Fig. 8 on the left part of the rightmost sector, on the left and right sides of the sector shown in the center, and on the beginning of the leftmost sector shown. There are also portions of these sectors which are covered by a grey layer. This layer may have appeared because of melting and/or evaporation of the gasket and glue which were used for sealing the Ti foils to the target frames before production of the target. The tempering colors seen in Fig. 8 indicate that temperature on the target frame could reach hundreds of degrees Celsius which could result in damage of the silicon gasket or glue.

The excitation energies stated previously were calculated assuming no material layer on the beam side of the target. If a layer is assumed the excitation energy is lowered. However, cross sections are calculated with the assumption of material blocking ER over some percent area of the target surface. This is derived from the alpha spectra measured. Calculations for ^{294}Og consider a reaction only as ^{48}Ca + ^{249}Cf and those for ^{296}Og only consider ^{48}Ca+^{251}Cf leading to a synthesis. For phase 1, it was assumed that 50 ± 20 percent of the target was not covered. This gives a cross-section for ^{294}Og of $0.9\,^{+3.2}_{-0.8}$ pb and places an upper limit for ^{296}Og of 3.4 pb. The given error bars and limit include statistical [46] as well as systematic uncertainties. During phase 2, it was assumed that $40\,^{+20}_{-15}$ percent of the target was not covered by material. The upper bounds for the cross-section are 4.1 pb for ^{294}Og and 5.7 pb for ^{296}Og.

In a similar way to previous publications [46, 51] we calculate the expectation value of the number of random events simulating a real event. The simulating event would be one with the following energies recorded in a DSSD pixel (with or without a corresponding event in

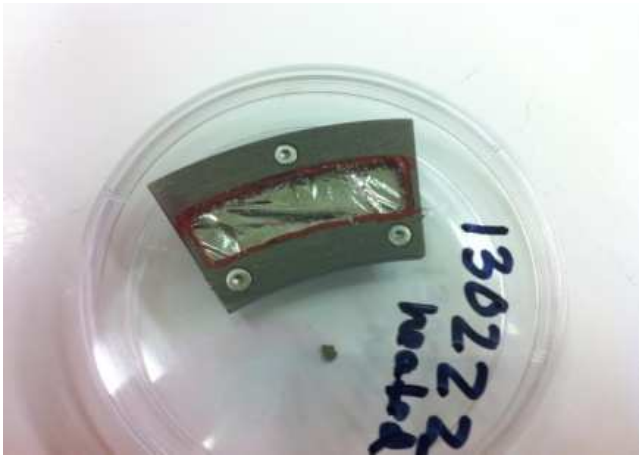

FIG. 7. Target wheel segment before irradiation.

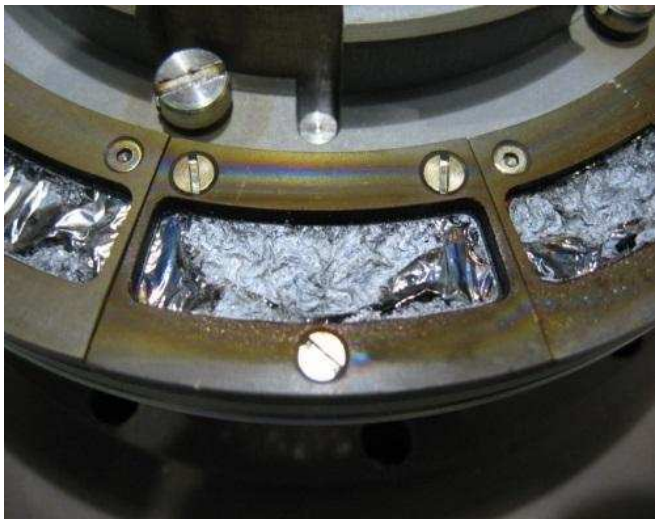

FIG. 8. Target wheel foil after irradiation.

the Si box): a TOF correlated recoil energy in the range of 4.5-18 MeV, with the first decay energy in the range of 11.2-12.2 MeV, followed by another in the range of 10.35-11.35 MeV, and terminating by an event simulating fission with an energy larger than 130 MeV. These events would need to occur relative to each other within the time intervals of 3 ms, 50 ms, and 600 ms, respectively. Using these criteria, the event assigned to ^{294}Og (observed during phase 1) and shown in Fig. 5 has an expected number of random events of about 10^{-11}.

V. FUTURE OUTLOOK

The mixed californium target material is currently being recovered and will be fabricated into new targets of a different design free from the silicon gasket and glue. The continuation of this experimental program is encouraged by previous experiments [10, 13, 14], the initial, quick success of the experiment producing ^{294}Og and cross-section and fission barrier predictions [17, 54] which show a cross-section of synthesizing ^{295}Og on the order of 1 pb. Furthermore, a microscopic-macroscopic approach by Adam Sobiczewski [55] and a recent systematic evaluation of a subset of models within the covariant density functional theory (CDFT) framework shows relative agreement between models in this region [56], and models further agree that fission barriers are not changing drastically for oganesson isotopes moving from $N = 176$ to $N = 178$. Therefore, it is reasonable to assert that since ^{294}Og was produced, it can be likely that ^{295}Og or ^{296}Og could yet be produced from this Cf material when it is recovered.

The current summary of various theoretical models for decay properties of ^{294}Og and ^{296}Og are shown in Fig. 9 along with the new average decay properties of $E_\alpha = 11.70 \pm 0.03$ MeV and $T_{1/2} = 0.58\ ^{+44}_{-18}$ ms. Listed in chronological order, these models agree that ^{294}Og could have a larger Q_α and shorter half-life than ^{296}Og. The isotope ^{296}Og is predicted to have an alpha decay energy between 10.5-12 MeV and a half-life between 0.1ms and 1s. From experimental extrapolation, one expects $E_\alpha \approx 11.45$ MeV and a half-life of a few milliseconds. This is well within our experimental sensitivity.

VI. CONCLUSIONS

Attempts to synthesize oganesson isotopes heavier than ^{294}Og have begun. Success was achieved in being able to synthesize the ^{294}Og for the fifth time and from a third target material. This unique mixed-Cf target illustrates the importance and difficulties associated with new and novel target materials. The mixed-Cf target also offers an increased experimental reach towards new superheavy nuclei. It has been shown that digital electronics can provide an additional tool for probing the shortest activities observable in the DGFRS. This system is further important for campaigns which will utilize higher beam intensities and due to the ability for short dead times, important for synthesizing elements with $Z>118$. Additionally, the isotopes of the next synthesized new elements may have very short half-lives in comparison to those approaching $N = 184$, where it is expected there is a region of enhanced stability of superheavy nuclei.

ACKNOWLEDGMENTS

We especially thank the personnel operating the U400 cyclotron, the associates of the ion-source group for obtaining intense ^{48}Ca beams and the REDC operators and technicians. This work is funded under the grants from the U.S. DOE Office of Nuclear Physics under DOE Contract No. DE-AC05-00OR22725 with UT Battelle, LLC and the Russian Foundation for Basic Research grant No. 16-52-55002. Research is further supported by LDRD

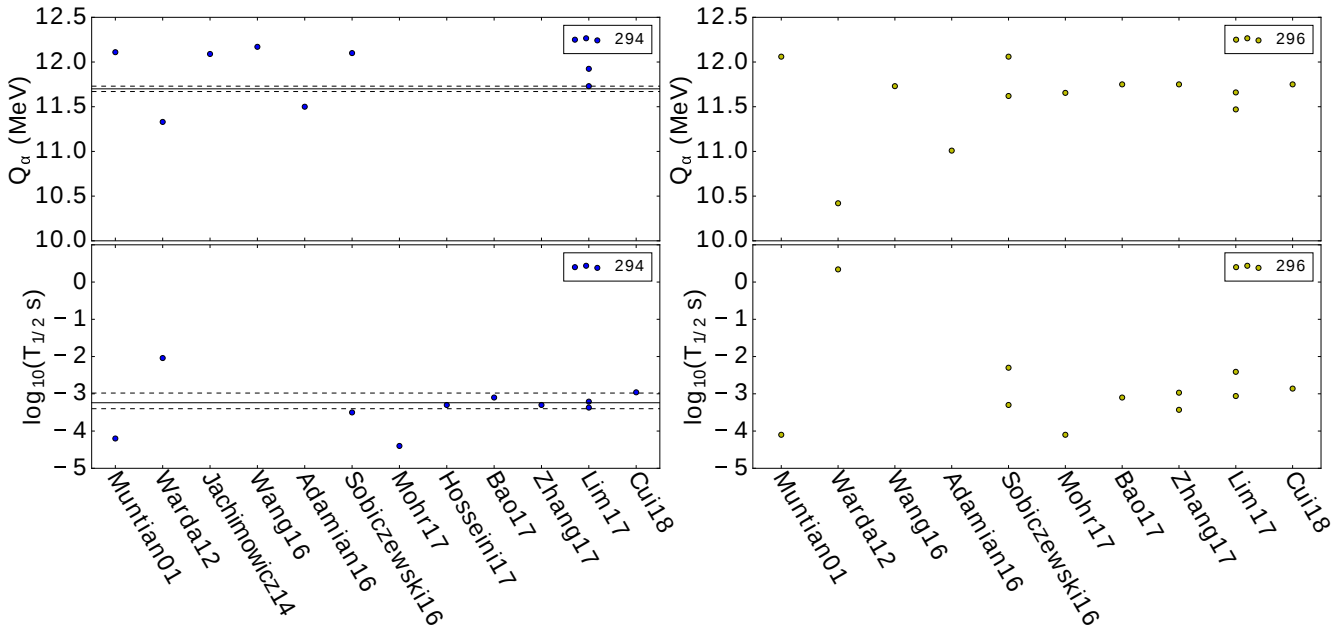

FIG. 9. The decay properties (Q_α (top) and $T_{1/2}$ (bottom)) of ^{294}Og (left) and ^{296}Og (right) from various theoretical approaches (chronologically ordered). The current average values and errors for ^{294}Og are shown as solid and dashed lines, respectively. The x-axis refers to references Muntian01 : [57], Warda12 : [58], Jachimowicz14 : [59], Wang16 : [60], Adamian16 : [25], Sobicziewski16 : [55], Mohr17 : [61], Hosseini17 : [62], Bao17 : [63], Zhang17 : [64], Lim17 : [65], and Cui18 : [66].

Program Project No. 08-ERD-030 and DOE Contract No, DE-AC52-07NA27344 with Lawrence Livermore National Security, LLC for research done at LLNL and by the U.S. DOE through Grant No. DE-FG-05-88ER40407 for contributions from Vanderbilt University.

VII. REFERENCES

[1] L. Öhrström and J. Reedijk, Pure Appl. Chem. **88**, 1225 (2016).
[2] Y. T. Oganessian and K. P. Rykaczewski, Phys. Today **68**, 32 (2015).
[3] Y. T. Oganessian and V. K. Utyonkov, Nucl. Phys. A **944**, 62 (2015).
[4] P. Pyykkö, Phys. Chem. Chem. Phys. **13**, 161 (2011).
[5] A. Baran, M. Kowal, P.-G. Reinhard, L. M. Robledo, A. Staszczak, and M. Warda, Nucl. Phys. A **944**, 442 (2015).
[6] P. Jerabek, B. Schuetrumpf, P. Schwerdtfeger, and W. Nazarewicz, Phys. Rev. Lett. **120**, 053001 (2018).
[7] B. Schuetrumpf, W. Nazarewicz, and P.-G. Reinhard, Phys. Rev. C **96**, 024306 (2017).
[8] W. Nazarewicz, Nature Physics **14**, 537 (2018).
[9] R. A. Boll, S. M. Van Cleve, N. J. Sims, L. K. Felker, J. D. Burns, G. D. Owen, E. H. Smith, C. S. White, and J. G. Ezold, J. Radioanal. Nucl. Chem. **305**, 921 (2015).
[10] Y. T. Oganessian, V. K. Utyonkov, Y. V. Lobanov, F. S. Abdullin, A. N. Polyakov, I. V. Shirokovsky, Y. S. Tsyganov, G. G. Gulbekian, S. L. Bogomolov, B. N. Gikal, *et al.*, Nucl. Phys. A **734**, 109 (2004).
[11] Y. T. Oganessian, V. K. Utyonkov, Y. V. Lobanov, F. S. Abdullin, A. N. Polyakov, I. V. Shirokovsky, Y. S. Tsyganov, G. G. Gulbekian, S. L. Bogomolov, B. N. Gikal, *et al.*, Phys. Rev. C **69**, 054607 (2004).
[12] Y. T. Oganessian, V. K. Utyonkov, Y. V. Lobanov, F. S. Abdullin, A. N. Polyakov, I. V. Shirokovsky, Y. S. Tsyganov, G. G. Gulbekian, S. L. Bogomolov, B. N. Gikal, *et al.*, Phys. Rev. C **70**, 064609 (2004).
[13] Y. T. Oganessian, V. K. Utyonkov, Y. V. Lobanov, F. S. Abdullin, A. N. Polyakov, R. N. Sagaidak, I. V. Shirokovsky, Y. S. Tsyganov, A. A. Voinov, G. G. Gulbekian, *et al.*, Phys. Rev. C **74**, 044602 (2006).
[14] Y. T. Oganessian, F. S. Abdullin, C. Alexander, J. Binder, R. A. Boll, S. N. Dmitriev, J. Ezold, K. Felker, J. M. Gostic, R. K. Grzywacz, *et al.*, Phys. Rev. Lett. **109**, 162501 (2012).
[15] J. Chen, I. Ahmad, J. P. Greene, and F. G. Kondev, Phys. Rev. C **90**, 044302 (2014).
[16] J. Zhang, C. Wang, and Z. Ren, Nucl. Phys. A **909**, 36 (2013).
[17] T. Cap, K. Siwek-Wilczyńska, M. Kowal, and J. Wilczyński, Phys. Rev. C **88**, 037603 (2013).

[18] P. Möller, J. R. Nix, W. D. Myers, and W. J. Swiatecki, At. Data Nucl. Data Tables **59**, 185 (1995).

[19] V. I. Zagrebaev and W. Greiner, Nucl. Phys. A **944**, 257 (2015).

[20] V. Zagrebaev and W. Greiner, Phys. Rev. C **78**, 034610 (2008).

[21] G. Mandaglio, G. Giardina, A. K. Nasirov, and A. Sobiczewski, Phys. Rev. C **86**, 064607 (2012).

[22] X. J. Bao, S. Q. Guo, H. F. Zhang, and J. Q. Li, J. Phys. G: Nucl. Part. Phys. **44**, 045105 (2017).

[23] M. Wang, G. Audi, F. G. Kondev, W. J. Huang, S. Naimi, and X. Xu, Chin. Phys. C **41**, 030003 (2017).

[24] X. J. Bao, Y. Gao, J. Q. Li, and H. F. Zhang, Phys. Rev. C **92**, 034612 (2015).

[25] G. G. Adamian, N. V. Antonenko, A. N. Bezbakh, and R. V. Jolos, Phys. Part. Nucl. **47**, 387 (2016).

[26] V. I. Zagrebaev, A. V. Karpov, and W. Greiner, Phys. Rev. C **85**, 014608 (2012).

[27] J. D. Burns, K. G. Myhre, N. J. Sims, D. W. Stracener, and R. A. Boll, Nucl. Inst. and Meth. A **830**, 95 (2016).

[28] K. Myhre, J. Burns, H. Meyer, N. Sims, and R. Boll, Surf. Sci. Spectra **23**, 70 (2016).

[29] J. B. Roberto, C. W. Alexander, R. A. Boll, J. D. Burns, J. G. Ezold, L. K. Felker, S. L. Hogle, and K. P. Rykaczewski, Nucl. Phys. A **944**, 99 (2015).

[30] M. N. Torrico, R. A. Boll, and M. Matos, Nucl. Inst. and Meth. A **790**, 64 (2015).

[31] V. K. Utyonkov, N. T. Brewer, Y. T. Oganessian, K. P. Rykaczewski, F. S. Abdullin, S. N. Dmitriev, R. K. Grzywacz, M. G. Itkis, K. Miernik, A. N. Polyakov, *et al.*, Phys. Rev. C **92**, 034609 (2015).

[32] Y. T. Oganessian, F. S. Abdullin, C. Alexander, J. Binder, R. A. Boll, S. N. Dmitriev, J. Ezold, K. Felker, J. M. Gostic, R. K. Grzywacz, *et al.*, Phys. Rev. C **87**, 054621 (2013).

[33] R. Grzywacz, Nucl. Inst. and Meth. B **204**, 649 (2003).

[34] R. Grzywacz, C. Gross, A. Korgul, S. Liddick, C. Mazzocchi, R. Page, and K. Rykaczewski, Nucl. Inst. and Meth. B **261**, 1103 (2007), the Application of Accelerators in Research and Industry.

[35] D. M. Miller and S. V. Paulauskas, www.github.com/pixie16/PixieSuite (2012).

[36] D. M. Miller, K. Miernik, N. T. Brewer, *et al.*, www.githib.com/ntbrewer/pixie_ldf_she (2015).

[37] K. Miernik, N. T. Brewer, and M. Shumeiko, www.githib.com/ntbrewer/pyspectr (2015).

[38] www.xia.com (2012).

[39] E. Browne and J. K. Tuli, Nucl. Data Sheets **112** (2011), data extracted from the ENSDF database (Nov. 30, 2014).

[40] M. D. Sun, Z. Liu, T. H. Huang, W. Q. Zhang, J. G. Wang, X. Y. Liu, B. Ding, Z. G. Gan, L. Ma, H. B. Yang, Z. Y. Zhang, L. Yu, J. Jiang, K. L. Wang, Y. S. Wang, M. L. Liu, Z. H. Li, J. Li, X. Wang, H. Y. Lu, C. J. Lin, L. J. Sun, N. R. Ma, C. X. Yuan, W. Zuo, H. S. Xu, X. H. Zhou, G. Q. Xiao, C. Qi, and F. S. Zhang, Phys. Lett. B **771**, 303 (2017).

[41] B. Singh and E. Browne, Nucl. Data Sheets **93** (2001), data extracted from the ENSDF database (Aug. 31, 2012).

[42] J. Khuyagbaatar, A. Yakushev, C. E. Düllmann, D. Ackermann, L.-L. Andersson, M. Block, H. Brand, D. M. Cox, J. Even, U. Forsberg, *et al.*, Phys. Rev. Lett. **115**, 242502 (2015).

[43] O. Häusser, W. Witthuhn, T. K. Alexander, A. B. McDonald, J. C. D. Milton, and A. Olin, Phys. Rev. Lett. **31**, 323 (1973).

[44] T. Nomura, K. Hiruta, T. Inamura, and M. Odera, Nucl. Phys. A **217**, 253 (1973).

[45] A. Chevallier, J. Chevallier, S. Khazrouni, L. Kraus, I. Linck, D. C. Radford, and N. Schulz, J. Physique **43**, 1597 (1982).

[46] K. H. Schmidt, C. C. Sahm, K. Pielenz, and H. G. Clerc, Z. Phys. A: At. Nucl. **316**, 19 (1984).

[47] K. H. Schmidt, Eur. Phys. J. A **8**, 141 (2000).

[48] E. K. Hulet, J. F. Wild, R. J. Dougan, R. W. Lougheed, J. H. Landrum, A. D. Dougan, P. A. Baisden, C. M. Henderson, R. J. Dupzyk, R. L. Hahn, M. Schädel, K. Sümmerer, and G. R. Bethune, Phys. Rev. C **40**, 770 (1989).

[49] D. C. Hoffman, M. M. Fowler, W. R. Daniels, H. R. Von Gunten, D. Lee, K. J. Moody, K. Gregorich, R. Welch, G. T. Seaborg, W. Brüchle, *et al.*, Phys. Rev. C **31**, 1763 (1985).

[50] Y. L. Zhang and Y. Z. Wang, Phys. Rev. C **97**, 014318 (2018).

[51] V. K. Utyonkov, N. T. Brewer, Y. T. Oganessian, K. P. Rykaczewski, F. S. Abdullin, S. N. Dmitriev, R. K. Grzywacz, M. G. Itkis, K. Miernik, A. N. Polyakov, J. B. Roberto, R. N. Sagaidak, I. V. Shirokovsky, M. V. Shumeiko, Y. S. Tsyganov, A. A. Voinov, V. G. Subbotin, A. M. Sukhov, A. V. Karpov, A. G. Popeko, A. V. Sabel'nikov, A. I. Svirikhin, G. K. Vostokin, J. H. Hamilton, N. D. Kovrizhnykh, L. Schlattauer, M. A. Stoyer, Z. Gan, W. X. Huang, and L. Ma, Phys. Rev. C **97**, 014320 (2018).

[52] F. Sauli, Nucl. Inst. and Meth. A **805**, 2 (2016).

[53] K. Miernik, in contribution to the 3rd Symposium on Super Heavy Elements - SHE 2017 Kazimierz Dolny, Poland (10-14 Sep. 2017).

[54] P. Jachimowicz, M. Kowal, and J. Skalski, Phys. Rev. C **95**, 014303 (2017).

[55] A. Sobiczewski, Phys. Rev. C **94**, 051302(R) (2016).

[56] S. E. Agbemava, A. V. Afanasjev, D. Ray, and P. Ring, Phys. Rev. C **95**, 054324 (2017).

[57] I. Muntian, Z. Patyk, and A. Sobiczewski, Acta Phys. Pol. B **32**, 691 (2001).

[58] M. Warda and J. L. Egido, Phys. Rev. C **86**, 014322 (2012).

[59] P. Jachimowicz, M. Kowal, and J. Skalski, Phys. Rev. C **89**, 024304 (2014).

[60] N. Wang, M. Liu, X. Wu, and J. Meng, Phys. Rev. C **93**, 014302 (2016).

[61] P. Mohr, Phys. Rev. C **95**, 011302(R) (2017).

[62] S. S. Hosseini and H. Hassanabadi, Chin. Phys. C **41**, 064101 (2017).

[63] X. J. Bao, S. Q. Guo, H. F. Zhang, and J. Q. Li, Phys. Rev. C **95**, 034323 (2017).

[64] S. Zhang, Y. L. Zhang, J. P. Cui, and Y. Wang, Phys. Rev. C **95**, 014311 (2017).

[65] Y. Lim and Y. Oh, Phys. Rev. C **95**, 034311 (2017).

[66] J. P. Cui, Y. L. Zhang, S. Zhang, and Y. Z. Wang, Phys. Rev. C **97**, 014316 (2018).